Les Houches school, Theoretical physics to face the challenge of LHC, August 2011

M.L. Mangano

CERN, PH-TH, 1211 Geneva 23, Switzerland

Contents

Part I

Week 4

1

Introduction to the theory of LHC collisions, by M.L.Mangano

1.1 Introduction

The frontier of high-energy physics is being redefined by the experiments at CERN's Large Hadron Collider (LHC), the proton-proton collider operating at a center of mass energy of 8 TeV (to become ~ 14 TeV by 2014). The main goal of these experiments is to unveil the nature of electroweak symmetry breaking, via the detection of the Higgs boson and of other new particles associated to possible extensions of the Standard Model (SM). While strong interactions between quarks and gluons — described by quantum chromodynamics (QCD) — have no direct relation to electroweak phenomena, their role in making the LHC physics programme possible cannot however be underestimated. The processes leading to the creation of Higgs bosons, and other interesting particles, are all driven by the interactions among quarks and gluons, and it is these interactions that will define the production rate of the new phenomena, as well as of the numerous SM processes that will act as irreducible backgrounds to their detection. A solid and quantitative understanding of the role of strong interactions in LHC physics is therefore essential for a full exploitation of the LHC discovery and measurement potential. Most of the collisions between the protons are the result of the complex long-distance QCD dynamics responsible for holding quarks together, and their quantitative description still lacks a robust first-principle understanding. On the other hand, the processes leading to the production of heavy elementary particles arise from the short-distance interactions among the pointlike proton constituents. These *hard* interactions can be described by the perturbative regime of QCD, making it possible to perform quantitative, first-principle predictions.

These lectures will illustrate the basic principles underlying the use of perturbative QCD in predicting the structure of hard processes in high-energy hadronic collisions. The starting point, in section 1.2, will be a discussion of the factorization formula, which is the basis for the description of all hard processes in terms of universal functions parametrizing the density of quarks and gluons inside the proton. In section 1.3 I discuss the evolution of the perturbative final states, made of quarks and gluons, toward physical systems made of hadrons. Finally, section 1.4 collects several applications and examples of comparisons between the theoretical predictions and the current data. These will provide a picture of the success of this theoretical framework, giving good confidence on the reliability of its future applications to the study of LHC collisions.

The treatment will be introductory, and the emphasis will be on basic and intuitive physics concepts. Given the large number of papers that contributed to the development of the field, it is impossible to provide a complete and fair bibliography. I therefore limit my bibliography to some review books, and to references to some of the key results discussed here. For an excellent description of the early ideas about quarks and their dynamics, the classic reference is Feynman's book (1). The emergence of QCD as a theory for strong interactions is nicely reviewed in (2). For a general, but rather formal, introduction to QCD, see, for example, Ref. (3). For a more modern and pedagogical introduction, in the context of an introductory course to field theory, I refer to the excellent book by Peskin and Schroeder (4). For a general introduction to collider physics, see Ref. (5). For QCD applications to LEP, Tevatron and LHC, see Ref. (6) and, specifically for the LHC, see Ref. (7). Explicit calculations, including the nitty-gritty details of next-to-leading-order (NLO) calculations and renormalization, are given in great detail for several concrete cases of interest in Ref. (8). Many of the ideas used in this review are inspired by the very physical perspective presented in Ref. (9). While I shall be making occasional reference to perturbative calculations and to Monte Carlo generator tools, I shall not provide a systematic review of the state of the art in these very active areas. For recent status reports, see (10; 11).

1.2 QCD and the proton structure at large Q^2

The understanding of the structure of the proton at short distances is one of the key ingredients to predict cross sections for processes involving hadrons in the initial state. All processes in hadronic collisions, even those intrinsically of electroweak nature such as the production of W/Z bosons or photons, are in fact induced by the quarks and gluons contained inside the hadron. In this section I shall introduce some important concepts, such as the notion of partonic densities of the proton, and of parton evolution. These are the essential tools used by theorists to predict production rates for hadronic reactions.

We shall limit ourselves to processes where a proton–(anti)proton pair collides at large centre-of-mass energy ($\sqrt{S}$, typically larger than several hundred GeV) and undergoes a very inelastic interaction, with momentum transfers between the participants in excess of several GeV. The outcome of this hard interaction could be the simple scattering at large angle of some of the hadron's elementary constituents, their annihilation into new massive resonances, or a combination of the two. In all cases the final state consists of a large multiplicity of particles, associated to the evolution of the fragments of the initial hadrons, as well as of the new states produced. As discussed below, the fundamental physical concept that makes the theoretical description of these phenomena possible is 'factorization', namely the ability to isolate separate independent phases of the overall collision. These phases are dominated by different dynamics, and the most appropriate techniques can be applied to describe each of them separately. In particular, factorization allows one to decouple the complexity of the proton structure and of the final-state hadron formation from the elementary nature of the perturbative hard interaction among the partonic constituents.

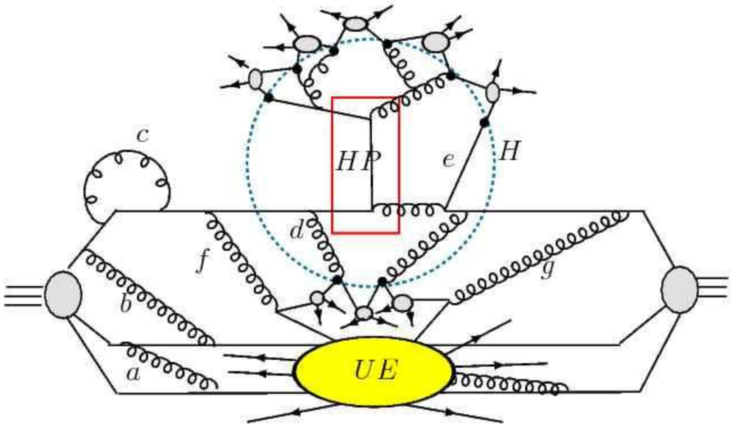

Fig. 1.1 General structure of a hard proton–proton collision

Figure 1.1 illustrates how this works. As the left proton travels freely before coming into contact with the hadron coming in from the right, its constituent quarks are held together by the constant exchange of virtual gluons (e.g. gluons a and b in the picture). These gluons are mostly soft, because any hard exchange would cause the constituent quarks to fly apart, and a second hard exchange would be necessary to reestablish the balance of momentum and keep the proton together. Gluons of high virtuality (gluon c in the picture) prefer therefore to be reabsorbed by the same quark, within a time inversely proportional to their virtuality, as prescribed by the uncertainty principle. The state of the quark is, however, left unchanged by this process. Altogether this suggests that the global state of the proton, although defined by a complex set of gluon exchanges between quarks, is nevertheless determined by interactions which have a time scale of the order of $1/m_p$. When seen in the laboratory frame where the proton is moving with energy $\sqrt{S}/2$, this time is furthermore Lorentz dilated by a factor $\gamma = \sqrt{S}/2m_p$. If we disturb a quark with a probe of virtuality $Q \gg m_p$, the time frame for this interaction is so short $(1/Q)$ that the interactions of the quark with the rest of the proton can be neglected. The struck quark cannot negotiate with its partners a coherent response to the external perturbation: it simply does not have the time to communicate to them that it is being kicked away. On this time scale, only gluons with energy of the order of Q can be emitted, something which, to happen coherently over the whole proton, is suppressed by powers of m_p/Q (this suppression characterizes the 'elastic form factor' of the proton). In the figure, the hard process is represented by the rectangle labelled HP. In this example a head-on collision with a gluon from the opposite hadron leads to a $qg \to qg$ scattering with a momentum exchange of the order of Q. This and other possible processes can be calculated from first principles in perturbative QCD, using elementary quarks and gluons as external states.

When the constituent is suddenly deflected, the partons that it had recently radiated cannot be reabsorbed (as happened to gluon c earlier) because the constituent is no longer there waiting for the partons to come back. This is the case, for example, of the gluon d emitted by the quark, and of the quark e from the opposite hadron; the emitted gluon got engaged in the hard interaction. The number of 'liberated' partons will depend on the hard scale Q: the larger the value of Q, the more sudden the deflection of the struck parton, and the fewer the partons that can reconnect before its departure (typically only partons with virtuality larger than Q).

After the hard process, the partons liberated during the evolution prior to the collision and the partons created by the hard collision will themselves emit radiation. The radiation process, governed by perturbative QCD, continues until a low virtuality scale is reached (the boundary region labelled with a dotted line, H, in our figure). To describe this perturbative evolution phase, proper care has to be taken to incorporate quantum coherence effects, which in principle connect the probabilities of radiation off different partons in the event. Once the low virtuality scale is reached, the memory of the hard-process phase has been lost, once again as a result of different time scales in the problem, and the final phase of hadronization takes over. Because of the decoupling from the hard-process phase, the hadronization is assumed to be independent of the initial hard process, and its parametrization, tuned to the observables of some reference process, can then be used in other hard interactions (universality of hadronization). Nearby partons merge into colour-singlet clusters (the grey blobs in fig. 1.1), which are then decayed phenomenologically into physical hadrons. To complete the picture, we need to understand the evolution of the fragments of the initial hadrons. As shown in the figure, this evolution cannot be entirely independent of what happens in the hard event, because at least colour quantum numbers must be exchanged to guarantee the overall neutrality and conservation of baryon number. In our example, the gluons f and g, emitted early on in the perturbative evolution of the initial state, split into $q\bar{q}$ pairs which are shared between the hadron fragments (whose overall interaction is represented by the oval labelled UE, for Underlying Event) and the clusters resulting from the evolution of the initial state.

The above ideas are embodied in the following factorization formula, which represents the starting point of any theoretical analysis of cross sections and observables in hadronic collisions:

$$\frac{d\sigma}{dX} = \sum_{j,k} \int_{\hat{X}} f_j(x_1, Q) f_k(x_2, Q) \, \frac{d\hat{\sigma}_{jk}(Q)}{d\hat{X}} \, F(\hat{X} \to X; Q) \, , \tag{1.1}$$

where:

- X is some hadronic observable (e.g. the transverse momentum of a pion, the invariant mass of a combination of particles, etc.);

- the sum over j and k extends over the partons types inside the colliding hadrons;
- the function $f_j(x, Q)$ (known as parton distribution function, PDF) parametrizes the number density of parton type j with momentum fraction x in a proton probed at a scale Q (more later on the meaning of this scale);
- $\hat{X}$ is a parton-level kinematical variable (e.g. the transverse momentum of a parton from the hard scattering);
- $\hat{\sigma}_{jk}$ is the parton-level cross section, differential in the variable $\hat{X}$;
- $F(\hat{X} \to X; Q)$ is a transition function, weighting the probability that the partonic state defining $\hat{X}$ gives rise, after hadronization, to the hadronic observable X.

In the rest of this Section I shall cover the above ideas in some more detail. While I shall not provide you with a rigorous proof of the legitimacy of this approach, I shall try to justify it qualitatively to make it sound at least plausible.

1.2.1 The parton densities and their evolution

As mentioned above, the binding forces responsible for the quark confinement are due to the exchange of rather soft gluons. If a quark were to exchange just a single hard virtual gluon with another quark, the recoil would tend to break the proton apart. It is easy to verify that the exchange of gluons with virtuality larger than Q is then proportional to some large power of m_p/Q, m_p being the proton mass. Since the gluon coupling constant gets smaller at large Q, exchange of hard gluons is significantly suppressed [1]. Consider in fact the picture in Fig. 1.2. The exchange of two gluons

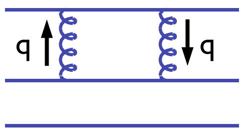

Fig. 1.2 Gluon exchange inside the proton

is required to ensure that the momentum exchanged after the first gluon emission is returned to the quark, and the proton maintains its structure. The contributions of hard gluons to this process can be approximated by integrating the loop over large momenta:

$$\int_Q \frac{d^4q}{q^6} \sim \frac{1}{Q^2} \,. \tag{1.2}$$

At large Q this contribution is suppressed by powers of $(m_p/Q)^2$, where the proton mass m_p is included as being the only dimensionful quantity available (one could use here the fundamental scale of QCD, Λ_{QCD}, but numerically this is anyway of the order of a GeV). The interactions keeping the proton together are therefore dominated by

[1] The fact that the coupling decreases at large Q plays a fundamental role in this argument. Were this not true, the parton picture could not be used!.

soft exchanges, with virtuality Q of the order of m_p. Owing to Heisenberg's uncertainty principle, the typical time scale of these exchanges is of the order of $1/m_p$: this is the time during which fluctuations with virtuality of the order of m_p can survive. In the laboratory system, where the proton travels with energy E, this time is Lorentz dilated to $\tau \sim \gamma/m_p = E/m_p^2$. If we probe the proton with an off-shell photon, the interaction takes place during the limited lifetime of the virtual photon, which, once more from the uncertainty principle, is given by the inverse of its virtuality. Assuming the virtuality $Q \gg m_p$, once the photon gets 'inside' the proton and meets a quark, the struck quark has no time to negotiate a coherent response with the other quarks, because the time scale for it to 'talk' to its partners is too long compared with the duration of the interaction with the photon itself. As a result, the struck quark has no option but to interact with the photon as if it were a free particle. Let us look in more detail

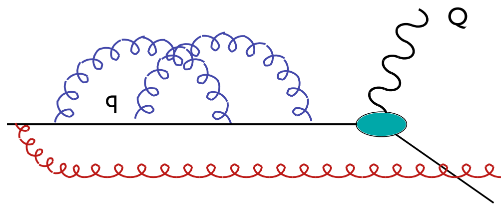

Fig. 1.3 Gluon emission at different scales during the approach to a hard collision.

at what happens during such a process. In Fig. 1.3 we see a proton as it approaches a hard collision with a photon of virtuality Q. Gluons emitted at a scale $q > Q$ have the time to be reabsorbed, since their lifetime is very short. Their contribution to the process can be calculated in perturbative QCD, since the scale is large and in the domain where perturbative calculations are meaningful. Since after being reabsorbed the state of the quark remains the same, their only effect is an overall renormalization of the wave function, and they do not affect the quark density. A gluon emitted at a scale $q < Q$, however, has a lifetime longer than the time it takes for the quark to interact with the photon, and by the time it tries to reconnect to its parent quark, the quark has been kicked away by the photon, and is no longer there. Since the gluon has taken away some of the quark momentum, the momentum fraction x of the quark as it enters the interaction with the photon is different than the momentum it had before, and therefore its density $f(x)$ is affected. Furthermore, when the scale q is of the order of 1 GeV the state of the quark is not calculable in perturbative QCD. This state depends on the internal wave function of the proton, which perturbative QCD cannot predict. We can, however, say that the wave function of the proton, and therefore the state of the 'free' quark, are determined by the dynamics of the soft-gluon exchanges inside the proton itself. Since the time scale of this dynamics is long relative to the time scale of the photon–quark interaction, we can safely argue that the photon sees to good approximation a static snapshot of the proton's inner configuration. In other words, the state of the quark had been prepared long before the photon arrived. This also suggests that the state of the quark will not depend on the precise nature of the external probe, provided the time scale of the hard interaction is very short compared to the time it would take for the quark to readjust itself. As a result, if we could perform some measurement of the quark state using, say, a virtual-photon probe, we could then use this knowledge on the state of the quark to perform predictions for the interaction of the proton with any other probe (e.g. a virtual W or even a gluon from an opposite beam of hadrons). This is the essence of the universality of the parton distributions.

The above picture leads to an important observation. It appears in fact that the distinction between which gluons are reabosrbed and which ones are not depends on the scale Q of the hard probe. As a result, the parton density $f(x)$ appears to depend on Q. This is illustrated in Fig. 1.4. The gluon emitted at a scale μ has a lifetime

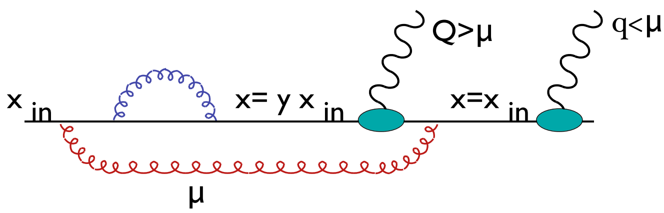

Fig. 1.4 Scale dependence of the gluon emission during a hard collision

short enough to be reabsorbed before a collision with a photon of virtuality $Q < \mu$, but too long for a photon of virtuality $Q > \mu$. When going from μ to Q, therefore, the partonic density $f(x)$ changes. We can easily describe this variation as follows:

$$f(x,Q) \;=\; f(x,\mu) + \int_x^1 dx_{in}\, f(x_{in},\mu) \int_\mu^Q dq^2 \int_0^1 dy\, P(y,q^2)\, \delta(x - yx_{in}) \;, \quad (1.3)$$

Here we obtain the density at the scale Q by adding to $f(x)$ at the scale μ (which we label as $f(x,\mu)$) all the quarks with momentum $x_{in} > x$ that retain a proton-momentum fraction $x = y/x_{in}$ by emitting a gluon. The function $P(y,Q^2)$ describes the 'probability' that the quark emits a gluon at a scale Q, keeping a fraction y of its momentum. This function does not depend on the details of the hard process, it simply describes the radiation of a free quark subject to an interaction with virtuality Q. Since $f(x,Q)$ does not depend upon μ (μ is just used as a reference scale to construct our argument), the total derivative of the right-hand side w.r.t. μ should vanish, leading to the following equation:

$$\frac{df(x,Q)}{d\mu^2} = 0 \quad \Rightarrow \frac{df(x,\mu)}{d\mu^2} \;=\; \int_x^1 \frac{dy}{y}\, f(y,\mu)\, P(x/y,\mu^2)\;. \quad (1.4)$$

Dimensional analysis and the fact that the gluon emission rate is proportional to the QCD coupling squared, allow us to further write:

$$P(x,Q^2) \;=\; \frac{\alpha_s}{2\pi}\frac{1}{Q^2}\, P(x) \quad (1.5)$$

from which the Dokshitzer–Gribov–Lipatov–Altarelli–Parisi (DGLAP) equation follows(12; 13; 14):

$$\frac{df(x,\mu)}{d\log\mu^2} = \frac{\alpha_s}{2\pi}\int_x^1 \frac{dy}{y}\, f(y,\mu)\, P_{qq}(x/y)\ . \tag{1.6}$$

The so-called *splitting function* $P_{qq}(x)$ can be calculated in perturbative QCD. The subscript qq is a labelling convention indicating that x refers to the momentum fraction retained by a quark after emission of a gluon.

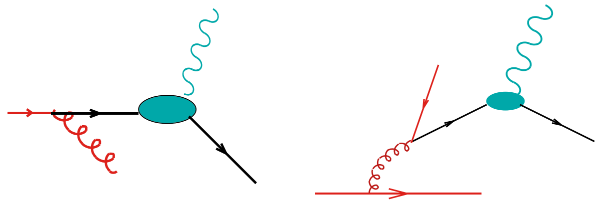

Fig. 1.5 The processes leading to the evolution of the quark density

More generally, one should consider additional processes. For example, one should include cases in which the quark interacting with the photon comes from the splitting of a gluon. This is shown in Fig. 1.5: the left diagram is the one we considered above; the right diagram corresponds to processes where an emitted gluon has the time to split into a $q\bar{q}$ pair, and it is one of these quarks which interacts with the photon. The overall evolution equation, including the effect of gluon splitting, is given by

$$\frac{dq(x,Q)}{dt} = \frac{\alpha_s}{2\pi}\int_x^1 \frac{dy}{y}\left[q(y,Q)\, P_{qq}(\frac{x}{y}) \ +\ g(y,Q)\, P_{qg}(\frac{x}{y})\right]\ , \tag{1.7}$$

where $t = \log Q^2$. For external probes that couple to gluons (for example an external

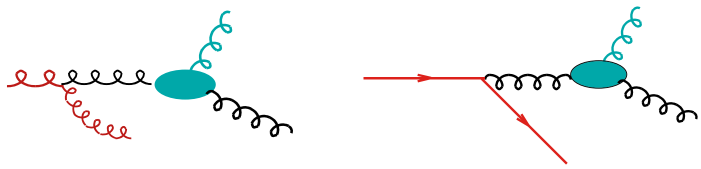

Fig. 1.6 The processes leading to the evolution of the gluon density

gluon, coming e.g. from an incoming proton), we have a similar evolution of the gluon density (see Fig. 1.6):

$$\frac{dg(x,Q)}{dt} = \frac{\alpha_s}{2\pi}\int_x^1 \frac{dy}{y}\left[g(y,Q)\, P_{gg}(\frac{x}{y}) \ +\ \sum_{q,\bar{q}} q(y,Q)\, P_{gq}(\frac{x}{y})\right]\ . \tag{1.8}$$

At the leading perturbative order (LO), the explicit calculation of the splitting functions $P_{ij}(x)$ (see, for example, Ref. (8)) gives then the following expressions[2]:

$$P_{qq}(x) = P_{gq}(1-x) = C_F \frac{1+x^2}{1-x} \tag{1.9}$$

$$P_{qg}(x) = \frac{1}{2}\left[x^2 + (1-x)^2\right] \tag{1.10}$$

$$P_{gg}(x) = 2C_A \left[\frac{1-x}{x} + \frac{x}{1-x} + x(1-x)\right] , \tag{1.11}$$

where $C_F = (N_C^2 - 1)/2N_C$ and $C_A = 2N_C$ are the Casimir invariants of the fundamental and adjoint representation of $SU(N_C)$ ($N_C = 3$ for QCD). In the following we shall derive some general properties of the PDF evolution, and give a few concrete examples.

The factorization given by eq.(1.1) cannot of course hold for all phenomena in hadronic collisions. Processes like elastic scattering or generic soft collisions cannot be described in terms of quarks and gluons, since they are driven by the long-distance structure of the proton. Furthermore, modifications to this simple factorization relation can be required to describe processes like hard diffraction. The DGLAP evolution of parton densities, furthermore, requires modifications with respect to what shown here when x is so small that $\alpha_s \log 1/x$ is of order 1, or when the gluon density becomes so large that gluon recombination becomes possible. Since the processes we shall consider in our applications do not cover these cases, we shall not further discuss these aspects in this review.

1.2.2 Example: quantitative evolution of parton densities

A complete solution for the evolved parton densities in x space can only be obtained from a numerical analysis. This work has been done by several groups (for a review see (15; 16)), and is continuously being updated (17; 18; 19; 20; 21) by including the most up-to-date experimental results used for the determination of the input densities at a fixed scale. The left side of fig. 1.7 shows the up-quark valence momentum density at various scales Q, as obtained from one of these studies. Note the softening at larger scales, and the clear $\log Q^2$ evolution. As Q^2 grows, the valence quarks emit more and more radiation, since they change direction over a shorter amount of time (larger acceleration). They therefore lose more momentum to the emitted gluons, and their spectrum becomes softer. The most likely momentum fraction carried by a valence up quark in the proton goes from $x \sim 20\%$ at $Q = 3$ GeV, to $x \lesssim 10\%$ at $Q = 1000$ GeV. Notice finally that the density vanishes at small x.

The right-hand side of fig. 1.7 shows the gluon momentum density. This grows at small x, with an approximate $g(x) \sim 1/x^{1+\delta}$ behaviour, and $\delta > 0$ slowly increasing

[2]The expressions given here are strictly valid only for $x \neq 1$. Slight modifications required to extend them to $x = 1$.

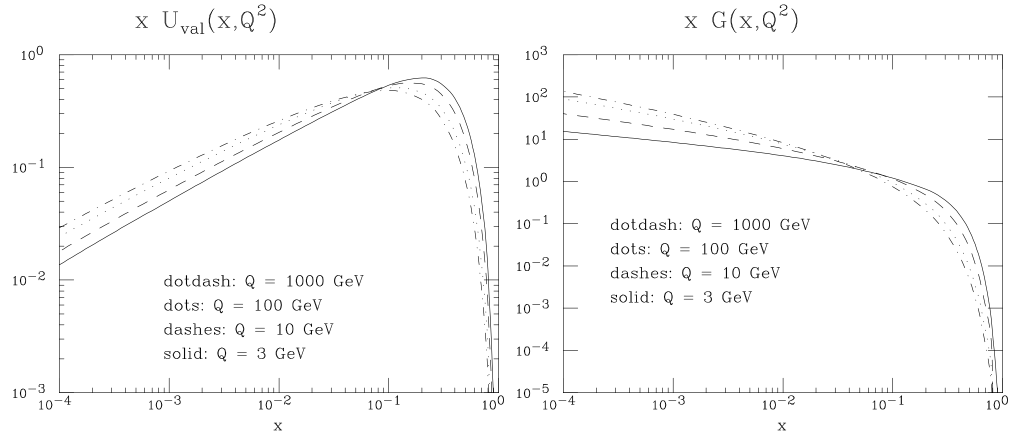

Fig. 1.7 Left: Valence up-quark momentum-density distribution, for different scales Q. Right: Gluon momentum-density distribution.

at large Q^2. This low-x growth is due to the $1/x$ emission probability for the radiation of gluons, which was discussed in the previous section and which is represented by the $1/x$ factors in the $P_{gq}(x)$ and $P_{gg}(x)$ splitting functions. As Q^2 grows we find an increasing number of gluons at small x, as a result of the increased radiation off quarks, as well as off the harder gluons.

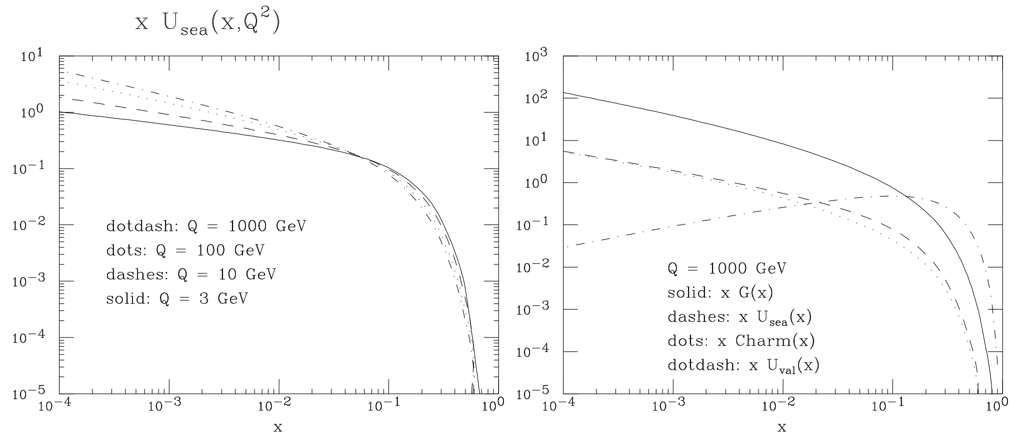

Fig. 1.8 Left: Sea up-quark momentum-density distribution, for different scales Q. Right: Momentum-density distribution for several parton species, at $Q = 1000$ GeV.

The left-hand side of Fig. 1.8 shows the evolution of the up-quark *sea* momentum density. Shape and evolution match those of the gluon density, a consequence of the fact that sea quarks come from the splitting of gluons. Since the gluon-splitting probability is proportional to α_s, the approximate ratio $sea/gluon \sim 0.1$, which can be obtained by comparing Figs. 1.7 and 1.8, is perfectly justified.

Finally, the momentum densities for gluons, up-sea, charm, and up-valence distributions are shown, for $Q = 1000$ GeV, on the right side of Fig.1.8. Note here that u_{sea} and charm are approximately the same at very large Q and small x, as will be discussed in more detail in the next subsection. The proton momentum is mostly carried by valence quarks and by gluons. The contribution of sea quarks is negligible.

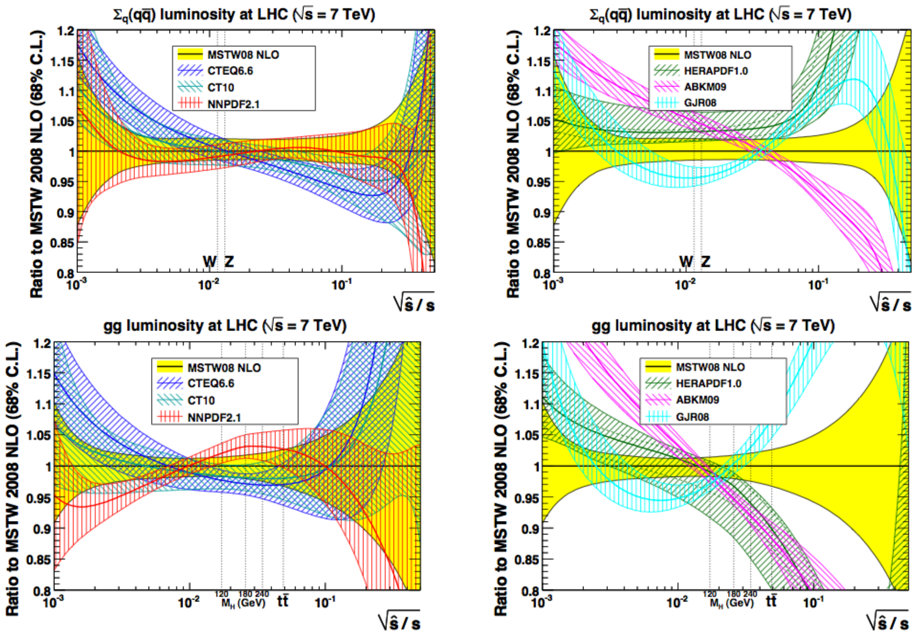

Fig. 1.9 Uncertainty in the parton luminosity functions at the LHC (22).

Parton densities are extracted from experimental data. Their determination is therefore subject to the statistical and systematic uncertainties of the experiments and of the theoretical analysis (e.g. the treatment of non-perturbative effects, the impact of missing higher-order perturbative corrections). Techniques have been introduced recently to take into account these uncertainties, and to evaluate their impact on concrete observables. A summary of such an analysis (22) is given in Figs. 1.9. What is plotted is the uncertainty bands for partonic luminosities[3] corresponding to the gg and $q\bar{q}$ initial-state channels. The partonic flux is given as a function of $\hat{s}$, the partonic CM invariant mass. Obvious features include the growth of uncertainty of the gg density at large mass, corresponding to the lack of data covering the large-x region of the gluon density. Notice, in particular, that the uncertainty bands reported by different groups do not necessarily overlap: this reflects different choices in the input

[3]For the definition of parton luminosity see Section 1.4.1.

sets of experimental data. In the future, the LHC data will be used in these global fits, leading to an important reduction in the uncertainties.

1.3 The final-state evolution of quarks and gluons

We discussed in the previous section the initial-state evolution of quarks and gluons as the proton approaches the hard collision. We study here how quarks and gluons evolve after emerging from the hard process, and finally transform into hadrons, neutralizing their colours. We start by considering the simplest case: e^+e^- collisions, which provide the cleanest environment in which to study applications of QCD at high energy. This is the place where theoretical calculations have today reached their best accuracy, and where experimental data are the most precise, especially thanks to the huge statistics accumulated by LEP, LEP2 and SLC. The key process is the annihilation of the e^+e^- pair into a virtual photon or Z^0 boson, which will subsequently decay to a $q\bar{q}$ pair. e^+e^- collisions have therefore the big advantage of providing an almost point-like source of quark pairs, so that, in contrast to the case of interactions involving hadrons in the initial state, we at least know very precisely the state of the quarks at the beginning of the interaction process.

Nevertheless, it is by no means obvious that this information is sufficient to predict the properties of the hadronic final state. We know that this final state is clearly not simply a $q\bar{q}$ pair, but some high-multiplicity set of hadrons. For example, as shown in Fig. 1.10, the average multiplicity of charged hadrons in the decay of a Z^0 is approximately 20. It is therefore not obvious that a calculation done using the simple picture

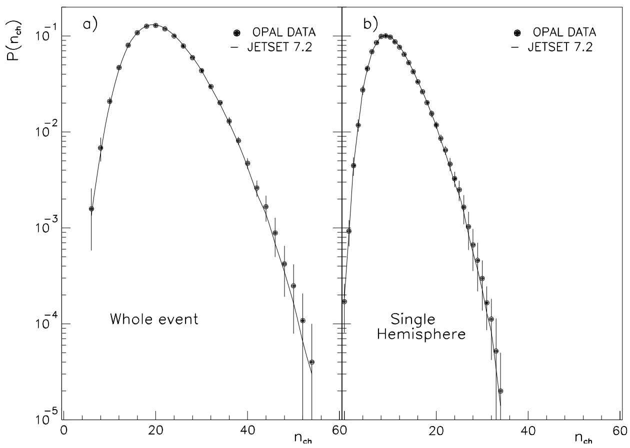

Fig. 1.10 Charged particle multiplicity distribution in Z^0 decays

$e^+e^- \to q\bar{q}$ has anything to do with reality. For example, one may wonder why we do not need to calculate $\sigma(e^+e^- \to q\bar{q}g\dots g\dots)$ for all possible gluon multiplicities to get an accurate estimate of $\sigma(e^+e^- \to \text{hadrons})$. And since in any case the final state is not made of q's and g's, but of π's, K's, ρ's, etc., why would $\sigma(e^+e^- \to q\bar{q}g\dots g)$ be enough?

The solution to this puzzle lies both in a question of time and energy scales, and in the dynamics of QCD. When the $q\bar{q}$ pair is produced, the force binding q and $\bar{q}$ is proportional to $\alpha_s(s)$ ($\sqrt{s}$ being the e^+e^- centre-of-mass energy). Therefore it is weak, and q and $\bar{q}$ behave to good approximation like free particles. The radiation emitted in the first instants after the pair creation is also perturbative, and it will stay so until a time after creation of the order of $(1\text{ GeV})^{-1}$, when radiation with wavelengths $\gtrsim (1\text{ GeV})^{-1}$ starts being emitted. At this scale the coupling constant is large, and non-perturbative phenomena and hadronization start playing a rôle. However, as we shall show, colour emission during the perturbative evolution organizes itself in such a way as to form colour-neutral, low-mass, parton clusters highly localized in phase-space. As a result, the complete colour-neutralization (i.e., the hadronization) does not involve long-range interactions between partons far away in phase-space. This is very important, because the forces acting among coloured objects at this time scale would be huge. If the perturbative evolution were to separate far apart colour-singlet $q\bar{q}$ pairs, the final-state interactions taking place during the hadronization phase would totally upset the structure of the final state.

In this picture, the identification of the perturbative cross section $\sigma(e^+e^- \to q\bar{q})$ with observable, high-multiplicity hadronic final states is realised by jets, namely collimated streams of hadrons that are the final result of the perturbative and non-perturbative evolution of each quark. The large multiplicity of the final states, shown

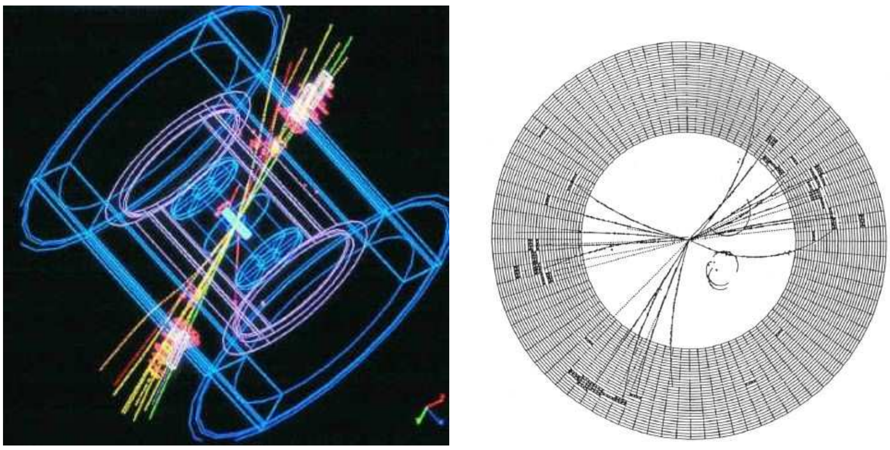

Fig. 1.11 Experimental pictures of 2- and 3-jet final states from e^+e^- collisions

in fig. 1.10, corresponds to the many particles that emerge from the collinear emissions of many gluons from each quark. The dynamics of these emissions leads these particles to grossly follow the direction of the primary quark, and the emergent bundle, the jet, inherits the kinematics of the initial quark. This is shown in the left image of fig. 1.11.

Three-jet events, shown in the right image of the figure, arise from the $O(\alpha_s)$ corrections to the tree-level process, namely to diagrams such as those shown in fig. 1.12.

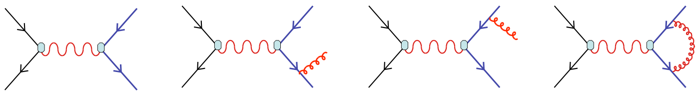

Fig. 1.12 $O(\alpha_s)$ corrections to the tree-level $e^+e^- \to q\bar{q}$ process

An important additional result of this 'pre-confining' evolution, is that the memory of where the local colour-neutral clusters came from is totally lost. So we expect the properties of hadronization to be universal: a model that describes hadronization at a given energy will work equally well at some other energy. Furthermore, so much time has passed since the original $q\bar{q}$ creation that the hadronization phase cannot significantly affect the total hadron production rate. Perturbative corrections due to the emission of the first hard partons should be calculable in PT, providing a finite, meaningful cross section.

The nature of non-perturbative corrections to this picture can be explored. One can prove, for example, that the leading correction to the total rate $R_{e^+e^-}$ is of order F/s^2, where $F \propto \langle 0|\alpha_s F^a_{\mu\nu} F^{\mu\nu a}|0\rangle$ is the so-called gluon condensate. Since $F \sim O(1 \text{ GeV}^4)$, these NP corrections are usually very small. For example, they are of $O(10^{-8})$ at the Z^0 peak. Corrections scaling like Λ^2/s or $\Lambda/\sqrt{s}$ can nevertheless appear in other less inclusive quantities, such as event shapes or fragmentation functions.

We now come back to the perturbative evolution, and shall devote the first part of this section to justifying the picture given above.

1.3.1 Soft gluon emission

Emission of soft gluons plays a fundamental rôle in the evolution of the final state (6; 9). Soft gluons are emitted with large probability, since the emission spectrum behaves like $\mathrm{d}E/E$, typical of bremsstrahlung as familiar in QED. They provide the seed for the bulk of the final-state multiplicity of hadrons. The study of soft-gluon emission is simplified by the simplicity of their couplings. Being soft (i.e., long wavelength) they are insensitive to the details of the very-short-distance dynamics: they cannot distinguish features of the interactions which take place on time scales shorter than their wavelength. They are also insensitive to the spin of the partons: the only feature they are sensitive to is the colour charge. To prove this let us consider soft-gluon emission in the $q\bar{q}$ decay of an off-shell photon:

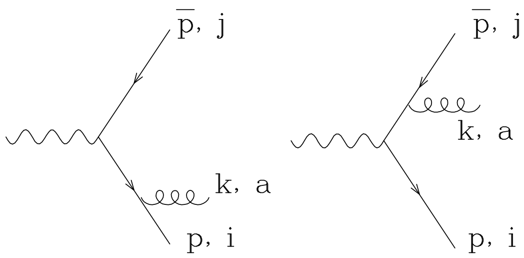

(1.12)

$$
\begin{aligned}
A_{soft} &= \bar{u}(p)\epsilon(k)(ig)\,\frac{-i}{\not{p}+\not{k}}\,\Gamma^\mu\, v(\bar{p})\ \lambda^a_{ij}\ +\ \bar{u}(p)\,\Gamma^\mu\,\frac{i}{\not{\bar{p}}+\not{k}}\,(ig)\epsilon(k)\,v(\bar{p})\ \lambda^a_{ij} \\
&= \left[\frac{g}{2p\cdot k}\,\bar{u}(p)\epsilon(k)\,(\not{p}+\not{k})\Gamma^\mu\, v(\bar{p})\ -\ \frac{g}{2\bar{p}\cdot k}\,\bar{u}(p)\,\Gamma^\mu\,(\not{\bar{p}}+\not{k})\epsilon(k)\,v(\bar{p})\right]\lambda^a_{ij}\ .
\end{aligned}
$$

I used the generic symbol Γ_μ to describe the interaction vertex with the photon to stress the fact that the following manipulations are independent of the specific form of Γ_μ. In particular, Γ_μ can represent an arbitrarily complicated vertex form factor. Neglecting the factors of $\not{k}$ in the numerators (since $k \ll p, \bar{p}$, by definition of soft) and using the Dirac equations, we get:

$$
A_{soft} = g\lambda^a_{ij}\ \left(\frac{p\cdot\epsilon}{p\cdot k} - \frac{\bar{p}\epsilon}{\bar{p}\cdot k}\right)\ A_{Born}\ . \tag{1.13}
$$

We then conclude that soft-gluon emission factorizes into the product of an emission factor, times the Born-level amplitude. From this exercise, one can extract general Feynman rules for soft-gluon emission:

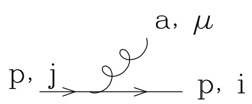

$$
= g\ \lambda^a_{ij}\ 2p^\mu\ . \tag{1.14}
$$

An analogous exercise leads to the $g \to gg$ soft-emission rules:

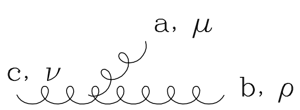

$$
= igf^{abc}\ 2p^\mu\ g^{\nu\rho}\ . \tag{1.15}
$$

Consider now the 'decay' of a virtual gluon into a quark pair. One more diagram should be added to those considered in the case of the electroweak decay. The fact that the quark pair is no longer in a colour-singlet state makes things a bit more interesting:

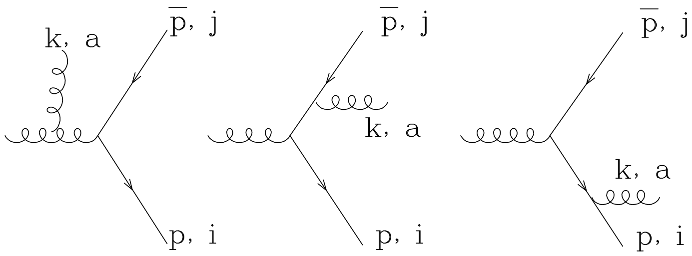

$$\stackrel{k\to 0}{=} \left[i\ g\ f^{abc}\ \lambda^c_{ij}\ \left(\frac{Q\epsilon}{Qk}\right) + g\ (\lambda^b\,\lambda^a)_{ij} \left(\frac{p\epsilon}{pk}\right) - g\ (\lambda^a\lambda^b)_{ij} \left(\frac{\bar{p}\epsilon}{pk}\right) \right] A_{Born}$$

$$= g\ (\lambda^a\,\lambda^b)_{ij} \left[\frac{Q\epsilon}{Qk} - \frac{\bar{p}\epsilon}{pk}\right] + g\ (\lambda^b\,\lambda^a)_{ij} \left[\frac{p\epsilon}{pk} - \frac{Q\epsilon}{Qk}\right] . \qquad (1.16)$$

The two factors correspond to the two possible ways colour can flow in this process:

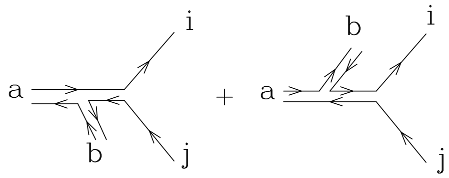

(1.17)

The basis for this representation of the colour flow is the following diagram which makes explicit the relation between the colours of the quark, antiquark, and gluon entering a QCD vertex:

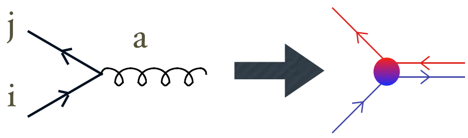

(1.18)

We can therefore represent the gluon as a double line, one line carrying the colour inherited from the quark, the other carrying the anticolour inherited from the antiquark. In the first diagram in (1.17) the antiquark (colour label j) is colour connected to the soft gluon (colour label b), and the quark (colour label i) is connected to the decaying gluon (colour label a). In the second case, the order is reversed. The two emission factors correspond to the emission of the soft gluon from the antiquark, and from the quark line, respectively. When squaring the total amplitude, and summing over initial and final-state colours, the interference between the two pieces is suppressed by $1/N^2$ relative to the individual squares:

$$\sum_{a,b,i,j} |(\lambda^a\lambda^b)_{ij}|^2 = \sum_{a,b} \mathrm{tr}\ \left(\lambda^a\lambda^b\lambda^b\lambda^a\right) = \frac{N^2-1}{2}\,C_F\ =\ O(N^3)\ . \qquad (1.19)$$

$$\sum_{a,b,i,j} (\lambda^a\lambda^b)_{ij}[(\lambda^b\lambda^a)_{ij}]^* = \sum_{a,b} \mathrm{tr}(\lambda^a\lambda^b\lambda^a\lambda^b) = \frac{N^2-1}{2} \underbrace{(C_F - \frac{C_A}{2})}_{-\frac{1}{2N}} = O(N) \tag{1.20}$$

As a result, the emission of a soft gluon can be described, to the leading order in $1/N^2$, as the incoherent sum of the emission from the two colour currents. The ability to separate these emissions as incoherent sums is the basic fact that allows a sequential, Markovian description of the parton-shower evolution as implemented in numerical simulations of the hadronic final state of hard collisions. The neglect of subleading $1/N^2$ contributions is therefore an intrinsic approximation of all such approaches.

1.3.2 Angular ordering for soft-gluon emission

The results presented above have important consequences for the perturbative evolution of the quarks. A key property of the soft-gluon emission is the so-called *angular ordering* (for an overview of colour-coherence and its relation to angular ordering, see (9; 23)). This phenomenon consists in the continuous reduction of the opening angle at which successive soft gluons are emitted by the evolving quark. As a result, this radiation is confined within smaller and smaller cones around the quark direction, and the final state will look like a collimated jet of partons. In addition, the structure of the colour flow during the jet evolution forces the $q\bar{q}$ pairs which are in a colour-singlet state to be close in phase-space, thereby achieving the pre-confinement of colour-singlet clusters alluded to at the beginning of this section.

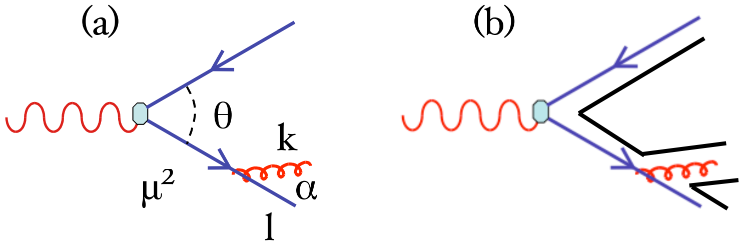

Fig. 1.13 Radiation off $q\bar{q}$ pair produced by an off-shell photon

A simple derivation of angular ordering, which more directly exhibits its physical origin, can be obtained as follows. Consider Fig. 1.13(a), which shows a Feynman diagram for the emission of a gluon from a quark line. The quark momentum is denoted by l and the gluon momentum by k, θ is the opening angle between the quark and antiquark, and α is the angle between the nearest quark and the emitted gluon. We shall work in the double-log enhanced soft $k^0 << l^0$ and collinear $\alpha << 1$ region. The internal quark propagator $p = (l + k)$ is off-shell, setting the time scale for the gluon emission:

$$\Delta t \simeq \frac{1}{\Delta E} = \frac{l^0}{(k+l)^2} \quad \to \quad \Delta t \simeq \frac{1}{k^0 \alpha^2} \, . \tag{1.21}$$

In order to resolve the quarks, the transverse wavelength of the gluon $\lambda_\perp = 1/E_\perp$ must be smaller than the separation between the quarks $b(t) \simeq \theta\,\Delta t$, giving the constraint $1/(\alpha k^0) < \theta\,\Delta t$. Using the results of Eq. 1.21 for Δt, we arrive at the angular ordering constraint $\alpha < \theta$. Gluon emissions at an angle smaller than θ can resolve the two individual colour quarks and are allowed; emissions at greater angles do not see the colour charge and are therefore suppressed. In processes involving more partons, the angle θ is defined not by the nearest parton, but by the colour connected parton (e.g. the parton that forms a colour singlet with the emitting parton). Figure 1.13(b) shows the colour connections for the $q\bar{q}$ event after the gluon is emitted. Colour lines begin on quarks and end on antiquarks. Because gluons are colour octets, they contain the beginning of one line and the end of another, as we showed in (1.17).

If one repeats now the exercise for emission of one additional gluon, one will find the same angular constraint, but this time applied to the colour lines defined by the previously established *antenna*. As shown in the previous subsection, the $q\bar{q}g$ state can be decomposed at the leading order in $1/N$ into two independent emitters, one given by the colour line flowing from the gluon to the quark, the other given by the colour line flowing from the antiquark to the gluon. So the emission of the additional gluon will be constrained to take place either within the cone formed by the quark and the gluon, or within the cone formed by the gluon and the antiquark. Either way, the emission angle will be smaller than the angle of the first gluon emission. This leads to the concept of angular ordering, with successive emission of soft gluons taking place within cones which get smaller and smaller, as in Fig. 1.14

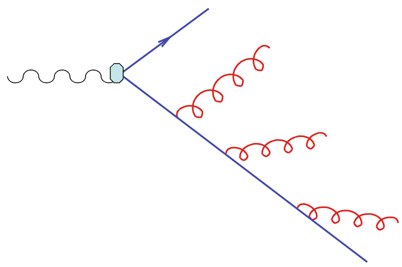

Fig. 1.14 Collimation of soft gluon emission during the jet evolution

The fact that colour always flows directly from the emitting parton to the emitted one, the collimation of the jet, and the softening of the radiation emitted at later stages, ensure that partons forming a colour-singlet cluster are close in phase-space. As a result, hadronization (the non-perturbative process that will bind together colour-singlet parton pairs) takes place locally inside the jet and is not a long-distance phenomenon connecting partons far away in the evolution tree: only pairs of nearby partons are involved. In particular, there is no direct link between the precise nature of the hard process and the hadronization. These two phases are totally decoupled and, as in the case of the partonic densities, one can infer that hadronization factorizes from the hard process and can be described in a universal (i.e. hard-process independent) fashion. The inclusive properties of jets (e.g. the particle multiplicity, jet mass, jet broadening) are independent of the hadronization model, up to corrections of order $(\Lambda/\sqrt{s})^n$ (for some integer power n, which depends on the observable), with $\Lambda \lesssim 1$ GeV.

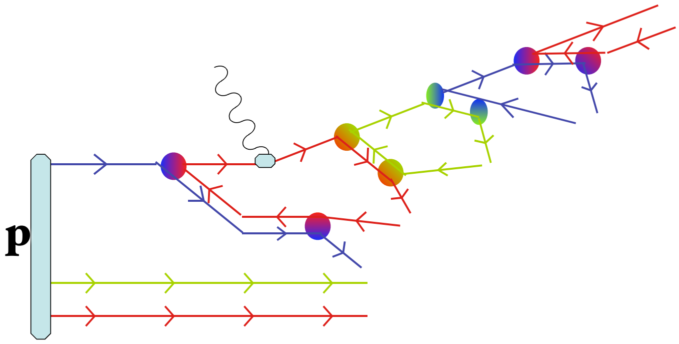

Fig. 1.15 The colour flow diagram for a DIS event

The final picture, in the case of a DIS event, appears therefore as in Fig. 1.15. After being deflected by the photon, the struck quark emits the first gluon that takes away the quark colour and passes on its own anticolour to the escaping quark. This gluon is therefore colour-connected with the last gluon emitted before the hard interaction. As the final-state quark continues its evolution, more and more gluons are emitted, each time leaving their colour behind and transmitting their anticolour to the emerging quark. Angular ordering forces all these gluons to be close in phase-space, until the evolution is stopped once the virtuality of the quark becomes of the order of the strong-interaction scale. The colour of the quark is left behind, and when hadronization takes over it is only the nearby colour-connected gluons which are transformed, with a phenomenological model, in hadrons. This mechanism for the transfer of colour across subsequent gluon emissions is similar to what happens when we place a charge near the surface of a dielectric medium. This will become polarized, and a charge will appear on the medium opposite end. The appearance of the charge is the result of a sequence of local charge shifts, whereby neighbouring atoms get polarized, as in Fig. 1.16. Notice

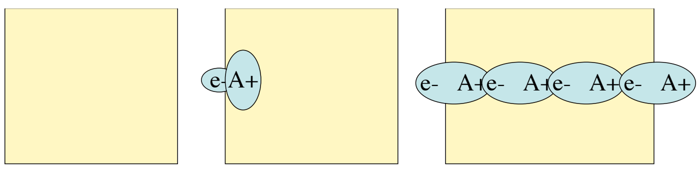

Fig. 1.16 Charge transfer in a dieletric medium, via a sequence of local polarizations

that the the transfer of colour between the final state jet and the jet associated to the initial state leads to the existence of one colour-singlet cluster containing partons from both jets. Therefore the particles arising from this cluster cannot be associated to either jet, they will be hadrons whose source is a combination of two of the hard partons in the event. This feature will be present in any hard process, it is the unavoidable consequence of the neutralization of the colour of the partons involved in the hard scattering.

1.3.3 Hadronization

The application of perturbation theory to the evolution of a jet, with the sequential emission of partons, governed by QCD splitting probabilities and angular ordering to enforce quantum mechanical quantum coherence, will stop once the scale of the emissions reaches values in the range of 1 GeV. This is called the *infrared cutoff*. The are two reasons why we need to stop the emission of gluons at this scale. To start with, we cannot control with perturbation theory the domain below this scale, where the strong coupling constant α_s becomes very large. Furthermore, we know that the number of physical particles that can be produced inside a jet must be finite, since the lightest object we can produce is a pion, and energy conservation sets a limit to how many pions can be created. This is different from what happens in a QED cascade, where the evolution of an accelerated charge can lead to the emission of an arbitrary number of photons. This is possible because the photon is massless, and can have arbitrarily small energy. The gluons of a QCD cascade, on the contrary, must have enough energy to create pions.

When the perturbative evolution of the jet terminates, we are left with some number of gluons. As shown in the previous subsection, and displayed in fig. 1.15, these gluons are pairwise colour connected. As two colour-connected gluons travel away from each other, a constant force pulls them together. Phenomenological models (see Ref. (6) for a more complete review) are then used to describe how this force determines the evolution of the system from this point on. What I shall describe here is the so-called *cluster model* (24), implemented in the HERWIG Monte Carlo generator (25; 26), but the main qualitative features are shared by other alternatives, such as the Lund string approach (27), implemented in the PYTHIA generator (28; 29).

Most of the hadrons emerging from the evolution of a jet are known to be made of quarks; glueballs, i.e. hadrons made of bound gluons, are expected to exist, but their production is greatly suppressed compared to that of quark-made particles. For this reason, the first step in the description of hadronization is to assume that the force among gluons will rip them apart into a $q\bar{q}$ pair, and that these quarks will act as seeds for the hadron production. The break-up into quarks is not parametrized using the DGLAP $g \to q\bar{q}$ splitting function, since we are deaing here with a non-perturbative transition. One typically employs therefore a pure phase-space 'decay' of the gluon into the $q\bar{q}$ pair, introducing as phenomenological parameters the relative probabilities of selecting the various active flavours (up, down, strange, etc.). The quark q_i from one gluon (i representing the flavour) then forms a colour-singlet pair with the antiquark $\bar{q}_j$ emerging from the break-up of the neighboring gluon. This colour-singlet $q_i\bar{q}_j$ pair cannot, however, directly form a hadron, since in general the quarks will still be moving apart, and the invariant mass of the pair will not coincide with the mass of an existing physical state. As they separate subject to a constant force, however, their kinetic

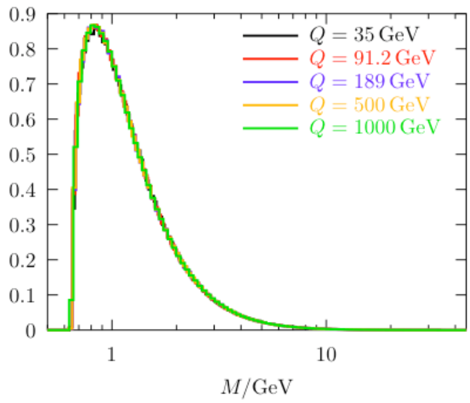

Fig. 1.17 Invariant mass distribution of clusters of colour-singlet quarks after non-perturbative gluon splitting, as obtained with the HERWIG generator (30). The spectra for final states corresponding to different centre-of-mass energies are normalized to the same area, displaying the energy independence of the shapes

energy turns into a linearly-rising potential energy. The potential energy accumulated in the system will be able to convert into a new quark–antiquark pair, $q_k\bar{q}_k$ once its value exceeds the relevant mass threshold. We are now left with two colour-singlet pairs, $q_i\bar{q}_k$ and $q_k\bar{q}_j$. When converting the potential energy into mass and kinetic energy of the newly produced pair, one can use the freedom in selecting the spatial kinematics of q_k and $\bar{q}_k$ such that both $q_i\bar{q}_k$ and $q_k\bar{q}_j$ invariant masses coincide with some resonance with the proper flavour. The residual energy of the system is then assumed to be entirely kinetic, and the two resonances fly away free. Once again, one can associate phenomenological parameters to the probabilities of selecting flavours k of a given type. Since the pair of flavour indices ik does not specify uniquely a hadron (e.g. a $u\bar{d}$ system could by a π^+, a ρ^+, as well as many other objects), the model has a further set of rules and/or parameters to select the precise flavour type. For example, a phenomenologically successfull description of the π/ρ ratio is obtained by simply assuming a production rate proportional to the number of spin states (one for the scalar pion, three for the vector rho) and to a Boltzmann factor $\exp(-M/T)$, where M is the resonance mass and T is a universal parameter, to be fit from data. Furthermore, one can introduce the possibility of converting the potential energy into a diquark–antidiquark pair, namely $(q_k q_\ell)\,(\bar{q}_k\bar{q}_\ell)$. The resulting hadrons, $q_i q_k q_\ell$ and $\bar{q}_j\bar{q}_k\bar{q}_\ell$ will be a baryon–antibaryon pair.

The measurement of hadron multiplicities from Z^0 decays is used to tune the few phenomenological parameters of the model, and these parameters can be used to describe hadronization at different energies and in different high-energy hadron-production processes. The internal consistency of this assumption is supported by fig. 1.17 (30), which shows the invariant mass distribution of clusters of colour-singlet quarks, after the non-perturbative gluon splitting, for e^+e^- collisions at different center-of-mass energies. All curves are normalized to 1, and they all overlap very accurately. This confirms the validity of the implementation of factorization in the Monte Carlo: higher initial energies provide more room for the perturbative evolution, leading to more splitting and more emitted radiation; but the structure and distribution of colour-singlet clusters at the end of evolution is independent of the initial energy, and the same model of hadronization can be applied.

1.4 Applications

In hadronic collisions, all phenomena are QCD related. The dynamics is more complex than in e^+e^- or DIS, since both beam and target have a non-trivial partonic structure. As a result, calculations (and experimental analyses) are more complicated. Perturbative corrections to the Born-level amplitudes (leading order, or LO) require the calculations of a large number of loop and high-order tree-level diagrams. For example, the first correction to the four LO $gg \to gg$ diagrams for the jet cross section in the purely gluonic channel requires the evaluation of the one-loop insertions in the four LO diagrams, plus the calculation of the 25 LO diagrams for the $gg \to ggg$ process. Next-to-leading-order (NLO) calculations like this are nevertheless available today for most processes with up to 2 or 3 final state partons, and new techniques have emerged recently that are pushing the frontier of NLO results even further (for a recent review see (10). Next-to-next-to-leading order (NNLO) results, which require the evaluation of two-loop corrections as well, have so far been completed only for processes with only one final-state particle at the Born level, such as production of massive gauge bosons (W, Z) or of a Higgs boson. For these reasons, the accuracy of QCD calculations in hadronic collisions is typically lesser than in the case of e^+e^- or DIS processes. Nevertheless, $p\bar{p}$ or pp collider physics is primarily *discovery* physics, rather than precision physics (there are exceptions, such as the measurements of the W mass and of the properties of b-hadrons. But these are not QCD-related measurements). As such, knowledge of QCD is essential both for the estimate of the expected signals, and for the evaluation of the backgrounds. Tests of QCD in $p\bar{p}$ collisions confirm our understanding of perturbation theory, or, when they fail, point to areas where our approximations need to be improved. (see, for example, the theory advances prompted by the measurements of ψ production at CDF).

In this section I shall briefly review some applications to the most commonly studied QCD processes in hadronic collisions: the production of gauge bosons and of jets. More details can be found in Refs. (6; 7).

1.4.1 Drell–Yan processes

While the Z boson has recently been studied with great precision by the LEP experiments, it was actually discovered, together with the W boson, by the CERN experiments UA1 and UA2 in $p\bar{p}$ collisions. W physics was studied in great detail at LEP2, but the best direct measurements of its mass by a single group still belong to $p\bar{p}$ experiments (CDF and D0 at the Tevatron). Until a new, future, e^+e^- linear collider will be built, the monopoly of W studies will remain in the hands of hadron colliders, with the Tevatron, and soon with the start of the LHC experiments.

Precision measurements of W production in hadronic collisions are important for several reasons:

- This is the only process in hadronic collisions which is known to NNLO accuracy.
- The rapidity distribution of the charged leptons from W decays is sensitive to the ratio of the up and down quark densities, and can contribute to our understanding of the structure of the proton.
- Deviations from the expected production rates of highly virtual W's ($p\bar{p} \to W^* \to e\nu$) are a possible signal of the existence of new W bosons, and therefore of new gauge interactions. The tail of the invariant mass distribution of the W, furthermore, provides today's most sensitive determination of the W width.

The production rate for the W boson is given by the factorization formula:

$$d\sigma(p\bar{p} \to W + X) = \int dx_1\ dx_2 \sum_{i,j} f_i(x_1, Q)\ f_j(x_2.Q)\ d\hat{\sigma}(ij \to W) \tag{1.22}$$

The partonic cross section $\hat{\sigma}(ij \to W)$ can be easily calculated, giving the following result (6; 5):

$$\hat{\sigma}(q_i\bar{q}_j \to W)\ =\ \pi\ \frac{\sqrt{2}}{3}\ |V_{ij}|^2\ G_F\ M_W^2\ \delta(\hat{s} - M_W^2)\ =\ A_{ij}\ M_W^2\ \delta(\hat{s} - M_W^2) \tag{1.23}$$

where $\hat{s}$ is partonic centre-of-mass energy squared, and V_{ij} is the element of the Cabibbo–Kobayashi–Maskawa matrix. The delta function comes from the $2 \to 1$ phase space, which forces the centre-of-mass energy of the initial state to coincide with the W mass. It is useful to introduce the two variables

$$\tau = \frac{\hat{s}}{S_{had}} \equiv x_1 x_2 \tag{1.24}$$

$$y = \frac{1}{2}\log\ \left(\frac{E_W + p_W^z}{E_W - p_W^z}\right) \equiv \frac{1}{2}\log\left(\frac{x_1}{x_2}\right)\ , \tag{1.25}$$

where S_{had} is the hadronic centre-of mass-energy squared. The variable y is called *rapidity.* For slowly moving objects it reduces to the standard velocity, but, contrary to the velocity, it transforms additively even at high energies under Lorentz boosts along the direction of motion. Written in terms of τ and y, the integration measure over the initial-state parton momenta becomes: $dx_1 dx_2 = d\tau dy$. Using this expression and Eq. (1.23) in Eq. (1.22), we obtain the following result for the LO total W production cross section:

$$\sigma_{DY} \;=\; \sum_{i,j} \frac{\pi\, A_{ij}}{M_W^2}\, \tau \int_\tau^1 \frac{dx}{x}\; f_i(x)\; f_j\left(\frac{\tau}{x}\right) \equiv \sum_{i,j} \frac{\pi\, A_{ij}}{M_W^2} \tau L_{ij}(\tau) \tag{1.26}$$

where the function $L_{ij}(\tau)$ is usually called *partonic luminosity*. In the case of $u\bar{d}$ collisions, the overall factor in front of this expression has a value of approximately 6.5 nb. It is interesting to study the partonic luminosity as a function of the hadronic centre-of-mass energy. This can be done by taking a simple approximation for the parton densities. Following the indications of the figures presented in the previous section, we shall assume that $f_i(x) \sim 1/x^{1+\delta}$, with $\delta < 1$. Then

$$L(\tau) \;=\; \int_\tau^1 \frac{dx}{x}\, \frac{1}{x^{1+\delta}} \left(\frac{x}{\tau}\right)^{1+\delta} = \frac{1}{\tau^{1+\delta}} \int_\tau^1 \frac{dx}{x} \;=\; \frac{1}{\tau^{1+\delta}}\; \log\left(\frac{1}{\tau}\right) \tag{1.27}$$

and

$$\sigma_W \sim \tau^{-\delta}\; \log\left(\frac{1}{\tau}\right) = \left(\frac{S_{had}}{M_W^2}\right)^\delta \log\left(\frac{S_{had}}{M_W^2}\right)\,. \tag{1.28}$$

The DY cross section grows therefore at least logarithmically with the hadronic centre-of-mass energy. This is to be compared with the behaviour of the Z production cross section in e^+e^- collisions, which is steeply diminishing for values of s well above the production threshold. The reason for the different behaviour in hadronic collisions is that while the energy of the hadronic initial state grows, it will always be possible to find partons inside the hadrons with the appropriate energy to produce the W directly on-shell. The number of partons available for the production of a W increases with the increase in hadronic energy, since the larger the hadron energy, the smaller will be the value of hadron momentum fraction x necessary to produce the W. The increasing number of partons available at smaller and smaller values of x causes then the growth of the total W production cross section.

A comparison between the best available predictions for the production rates of W and Z bosons in hadronic collisions and the LHC experimental data(31), is shown in Fig. 1.18. The experimental uncertainty is already smaller than the spread of the predictions based on different PDF sets, and will therefore add important constraints to improving the knowledge of PDFs.

Since the LHC is a pp collider, the initial state contains more up quarks than down quarks, and therefore the production rates and the distributions of W^+ bosons will be different than those of W^- bosons. For the total rates, this is well visible in Fig. 1.18. The rapidity asymmetry between positive and negative leptons produced in $W^\pm$ decays is shown in Fig. 1.19, where the ATLAS data are compared against the predictions of several PDF sets. Once again, the precision of the data strongly constrains the PDFs.

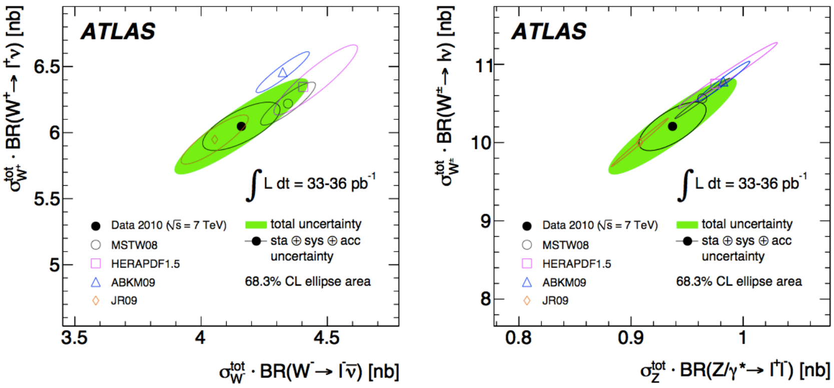

Fig. 1.18 Comparison of W and Z cross sections measured by the ATLAS experiment at the LHC (31), with the predictions of several PDF sets.

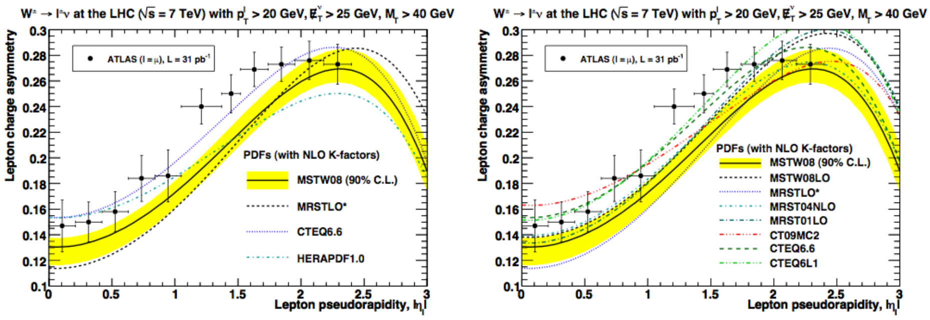

Fig. 1.19 The lepton charge asymmetry at the LHC, compared to the predictions of various PDF sets (22).

1.4.2 Jet production

Jet production is the hard process with the largest rate in hadronic collisions. The measurement of highest energy jets allows one to probe the shortest distances ever reached. The leading mechanisms for jet production are shown in fig. 1.20.

The 2-jet inclusive cross section can be obtained from the formula

$$d\sigma = \sum_{ijkl} dx_1\, dx_2\, f_i^{(H_1)}(x_1,\mu)\, f_j^{(H_2)}(x_2,\mu)\, \frac{d\hat{\sigma}_{ij\to k+l}}{d\Phi_2}\, d\Phi_2 \tag{1.29}$$

that has to be expressed in terms of the rapidity and transverse momentum of the quarks (or jets), in order to make contact with physical reality. The two-particle phase space is given by

$$d\Phi_2 = \frac{d^3k}{2k^0(2\pi)^3}\, 2\pi\, \delta((p_1+p_2-k)^2)\,, \tag{1.30}$$

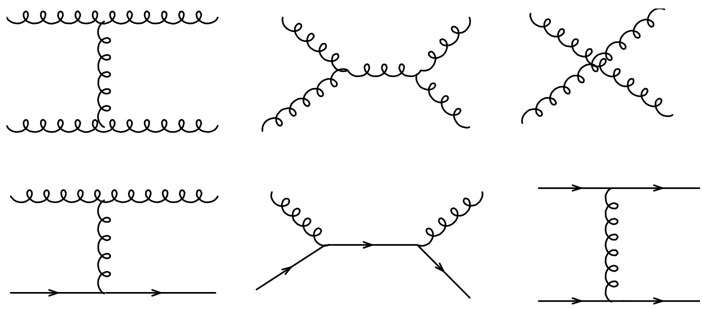

Fig. 1.20 Representative diagrams for the production of jet pairs in hadronic collisions

and, in the centre-of-mass of the colliding partons, we get

$$d\Phi_2 = \frac{1}{2(2\pi)^2}\, d^2k_T\, dy\, 2\,\delta(\hat{s} - 4(k^0)^2\,)\;, \tag{1.31}$$

where k_T is the transverse momentum of the final-state partons. Here y is the rapidity of the produced parton in the parton centre-of-mass frame. It is given by

$$y = \frac{y_1 - y_2}{2} \tag{1.32}$$

where y_1 and y_2 are the rapidities of the produced partons in the laboratory frame (in fact, in any frame). One also introduces

$$y_0 = \frac{y_1 + y_2}{2} = \frac{1}{2}\log\frac{x_1}{x_2}\;, \qquad \tau = \frac{\hat{s}}{S_{had}} = x_1\, x_2\;. \tag{1.33}$$

We have

$$dx_1\, dx_2 = dy_0\, d\tau\;. \tag{1.34}$$

We obtain

$$d\sigma = \sum_{ijkl} dy_0\, \frac{1}{S_{had}}\, f_i^{(H_1)}(x_1,\mu)\, f_j^{(H_2)}(x_2,\mu)\, \frac{d\hat{\sigma}_{ij\to k+l}}{d\Phi_2}\, \frac{1}{2(2\pi)^2}\, 2\, dy\, d^2k_T \tag{1.35}$$

which can also be written as

$$\frac{d\sigma}{dy_1\, dy_2\, d^2k_T} = \frac{1}{S_{had}\, 2(2\pi)^2} \sum_{ijkl} f_i^{(H_1)}(x_1,\mu)\, f_j^{(H_2)}(x_2,\mu)\, \frac{d\hat{\sigma}_{ij\to k+l}}{d\Phi_2}\;. \tag{1.36}$$

The variables x_1, x_2 can be obtained from y_1, y_2 and k_T from the equations

$$y_0 = \frac{y_1 + y_2}{2} \tag{1.37}$$

$$y = \frac{y_1 - y_2}{2} \tag{1.38}$$

$$x_T = \frac{2k_T}{\sqrt{S_{had}}} \tag{1.39}$$

$$x_1 = x_T\, e^{y_0}\, \cosh y \tag{1.40}$$
$$x_2 = x_T\, e^{-y_0}\, \cosh y\ . \tag{1.41}$$

For the partonic variables, we need $\hat{s}$ and the scattering angle in the parton centre-of-mass frame θ, since

$$t = -\frac{\hat{s}}{2}\,(1-\cos\theta)\,, \qquad u = -\frac{\hat{s}}{2}\,(1+\cos\theta)\,. \tag{1.42}$$

Neglecting the parton masses, you can show that the rapidity can also be written as:

$$y = -\log\tan\frac{\theta}{2} \equiv \eta\ , \tag{1.43}$$

with η usually being referred to as pseudorapidity.

The leading-order Born cross sections for parton–parton scattering are reported in Table 1.1.

Table 1.1 cross sections for light parton scattering. The notation is $p_1\,p_2 \;\to\; k\,l$, $\hat{s}=(p_1+p_2)^2$, $\hat{t}=(p_1-k)^2$, $\hat{u}=(p_1-l)^2$.

Process	$\frac{d\hat{\sigma}}{d\Phi_2}$
$qq' \to qq'$	$\frac{1}{2\hat{s}}\frac{4}{9}\frac{\hat{s}^2+\hat{u}^2}{\hat{t}^2}$
$qq \to qq$	$\frac{1}{2}\frac{1}{2\hat{s}}\left[\frac{4}{9}\left(\frac{\hat{s}^2+\hat{u}^2}{\hat{t}^2}+\frac{\hat{s}^2+\hat{t}^2}{\hat{u}^2}\right)-\frac{8}{27}\frac{\hat{s}^2}{\hat{u}\hat{t}}\right]$
$q\bar{q} \to q'\bar{q}'$	$\frac{1}{2\hat{s}}\frac{4}{9}\frac{\hat{t}^2+\hat{u}^2}{\hat{s}^2}$
$q\bar{q} \to q\bar{q}$	$\frac{1}{2\hat{s}}\left[\frac{4}{9}\left(\frac{\hat{s}^2+\hat{u}^2}{\hat{t}^2}+\frac{\hat{t}^2+\hat{u}^2}{\hat{s}^2}\right)-\frac{8}{27}\frac{\hat{u}^2}{\hat{s}\hat{t}}\right]$
$q\bar{q} \to gg$	$\frac{1}{2}\frac{1}{2\hat{s}}\left[\frac{32}{27}\frac{\hat{t}^2+\hat{u}^2}{\hat{t}\hat{u}}-\frac{8}{3}\frac{\hat{t}^2+\hat{u}^2}{\hat{s}^2}\right]$
$gg \to q\bar{q}$	$\frac{1}{2\hat{s}}\left[\frac{1}{6}\frac{\hat{t}^2+\hat{u}^2}{\hat{t}\hat{u}}-\frac{3}{8}\frac{\hat{t}^2+\hat{u}^2}{\hat{s}^2}\right]$
$gq \to gq$	$\frac{1}{2\hat{s}}\left[-\frac{4}{9}\frac{\hat{s}^2+\hat{u}^2}{\hat{s}\hat{u}}+\frac{\hat{u}^2+\hat{s}^2}{\hat{t}^2}\right]$
$gg \to gg$	$\frac{1}{2}\frac{1}{2\hat{s}}\frac{9}{2}\left(3-\frac{\hat{t}\hat{u}}{\hat{s}^2}-\frac{\hat{s}\hat{u}}{\hat{t}^2}-\frac{\hat{s}\hat{t}}{\hat{u}^2}\right)$

1.4.3 Comparison of theory and experimental data

Predictions for jet production at colliders are available today at the next-to-leading order in QCD (see the review in Ref. (7)). One of the preferred observables is the inclusive E_T spectrum. The agreement between data and theory at the LHC is excellent, as shown in Fig. 1.21. An accurate comparison of data and theory, should it exhibit discrepancies at the largest values of E_T, could provide evidence for new phenomena, such as the existence of a quark substructure (33). But how do we know that these discrepancies are not due to poorly known quark or gluon densities at large x? In

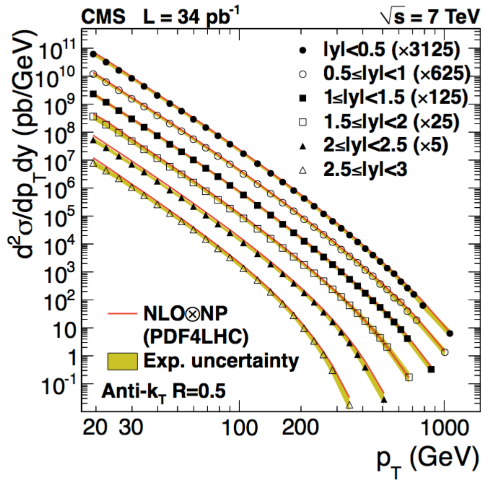

Fig. 1.21 Data vs. theory comparison for the inclusive jet spectrum measured by the CMS experiment at the LHC (32).

principle one could incorporate the jet data into a global fit to the partonic PDFs, and verify whether it is possible to modify them so as to maintain agreement with the other data, and at the same time to also fit satisfactorily the jet data themselves. On the other hand, doing this would prevent us from using the jet spectrum as a probe of new physics. In other words, we might be hiding away a possible signal of new physics by ascribing it to the PDFs. Is it possible to have a complementary determination of the PDF at high-x, that could constrain the possible PDF systematics of the jet cross section and at the same time leave the high-E_T tail as an independent and usable observable? This is indeed possible, by fully exploiting the kinematics of dijet production and the wide rapidity coverage of the collider detectors. One could in fact consider final states where the dijet system is highly boosted in the forward or backward region. For example, one could consider cases where $x_1 \to 1$ and $x_2 \ll 1$. In this case, the invariant mass of the dijet system would be small (since $M^2_{jj} = x_1 x_2 S \ll S$), and we know from lower-energy measurements that at this scale jets must behave like pointlike particles, following exactly the QCD-predicted rate. These final states are characterized by having jets at large positive rapidity. One can therefore perform a measurement with forward jets, and use these data to fit the $x_1 \to 1$ behaviour of the quark and gluon PDFs without the risk of washing away possible new-physics effects. At that point, the large-x PDFs thus constrained can be safely applied to the kinematical configurations where both x_1 and x_2 are large, namely the highest-E_T final states, and, if any residual discrepancy between data and theory is observed, infer the possible presence of new physics. The agreement seen in Fig. 1.21 in the data at large rapidity suggests that the PDF parameterizations at large x are reliable. A closer study of correlations among the two leading jets in the events can then lead to strong constraints on the possible composite structure of quarks, as seen for example in the ATLAS study of Ref. (34).

Of great phenomenological interest, in particular in the context of the study of backgrounds to the production of top quarks, of the Higgs boson, and of several signals of new physics, is the associated production of W or Z bosons and jets. LHC data and theoretical predictions are so far in very good agreement, as shown in Fig. 1.22. Similar

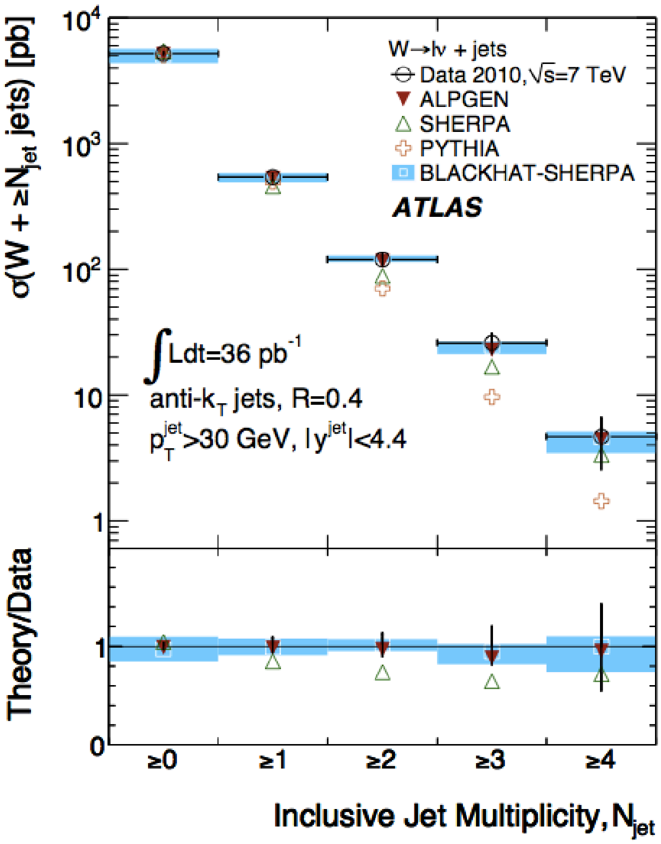

Fig. 1.22 Production rates of W plus multijets, measured by ATLAS at the LHC (35), compared against various theoretical predictions.

excellent agreement between data and QCD has been observed for a large number of observables, ranging from the inner structure of jets, to the spectra of high-p_T photons, to the production rates of bottom and top quarks.

1.5 Outlook and conclusions

In spite of the intrinsic complexity of the proton, the factorization framework allows a complete, accurate and successfull description of the rates and properties of hard processes in hadronic collisions. One of the key ingredients of this formulation is the universality of the phenomenological parametrizations of the various non-perturbative components of the calculations (the partonic densities and the hadronization phase). This universality makes it possible to extract the non-perturbative information from the comparison of data and theory in a set of benchmark measurements, and to apply this knowledge to different observables, or to different experimental environments. All the differences will be then accounted for by the purely perturbative part of the evolution.

Many years of experience at the Tevatron collider, at HERA, and at LEP, have led to an immense improvement of our understanding, and to the validation, of this framework, and put us today in a solid position to reliably anticipate in quantitative terms the features of LHC final states. LEP, in addition to testing with great accuracy the electroweak interaction sector, has verified at the percent level the predictions of perturbative QCD, from the running of the strong coupling constant, to the description of the perturbative evolution of single quarks and gluons, down to the non-perturbative boundary where strong interactions take over and cause the confinement of partons into hadrons. The description of this transition, relying on the factorization theorem that allows to consistently separate the perturbative and non-perturbative phases, has been validated by the study of LEP data at various energies, and their comparison with data from lower-energy e^+e^- collider, allowing the phenomenological parameters introduced to model hadronization to be determined. The factorization theorem supports the use of these parameters for the description of the hadronization transition in other experimental environments. HERA has made it possible to probe with great accuracy the short-distance properties of the proton, with the measurement of its partonic content over a broad range of momentum fractions x. These inputs, from LEP and from HERA, beautifully merge into the tools that have been developed to describe proton-antiproton collisions at the Tevatron, where the agreement between theoretical predictions and data confirms that the key assumptions of the overall approach are robust.

The accuracy of the perturbative input relies on complete higher-order calculations, as well as possible resummations of leading contributions to all orders of perturbation theory. Today's theoretical precision varies form the few per cent level of W and Z inclusive cross sections, which are known to next-to-next-to-leading order, to the level of 10% for several processes known to next-to-leading-order (inclusive jet cross sections, top quark production, production of pairs of electroweak gauge bosons), up to very crude estimates for the most complex, multijet final states, where uncertainties at the available leading-order can be as large as factors of 2 or more. At the LHC, the statistics and systematics for measurements like the total W, Z or $t\bar{t}$ cross sections are expected to be reduced to the few per cent level, comparable to the theoretical accuracy. These measurements, and others, will allow us to stress-test our modeling of basic phenomena at the LHC and to validate and improve their reliability, laying the fundations for a successfull exploration of the new landscapes that will be uncovered at the energy frontier.

References

[1] R.P. Feynman, Photon–Hadron Interactions (W.A. Benjamin, New York, 1972).
[2] D.J. Gross, hep-th/9809060; G. 't Hooft, hep-th/9808154.
[3] T. Muta, Foundations of QCD (World Scientific, Singapore, 1998).
[4] M.E. Peskin and D.V. Schroeder, An Introduction to Quantum Field Theory (Addison-Wesley, Reading, MA, 1995).
[5] V. Barger and R.J.N. Phillips, Collider Physics (Addison-Wesley, Redwood City, CA, 1997).
[6] R.K. Ellis, W.J. Stirling and B.R. Webber, QCD and Collider Physics (Cambridge University Press, 1996).
[7] J. M. Campbell, J. W. Huston and W. J. Stirling, Rep. Prog. Phys. **70** (2007) 89 [arXiv:hep-ph/0611148].
[8] R. Field, Applications of Perturbative QCD (Addison-Wesley, Redwood City, CA, 1989).
[9] Yu.L. Dokshitzer, V.A. Khoze, A.H. Mueller and S.I. Troyan, Basics of Perturbative QCD (Editions Frontières, Gif-sur-Yvette, 1991).
[10] L. J. Dixon, arXiv:0712.3064 [hep-ph].
[11] M. A. Dobbs *et al.*, arXiv:hep-ph/0403045.
[12] V. N. Gribov and L. N. Lipatov, Sov. J. Nucl. Phys. **15** (1972) 438 [Yad. Fiz. **15** (1972) 781].
[13] G. Altarelli and G. Parisi, Nucl. Phys. B **126** (1977) 298.
[14] Y. L. Dokshitzer, Sov. Phys. JETP **46** (1977) 641 [Zh. Eksp. Teor. Fiz. **73** (1977) 1216].
[15] M. Dittmar *et al.*, arXiv:0901.2504 [hep-ph].
[16] H. Jung *et al.*, arXiv:0903.3861 [hep-ph].
[17] P. M. Nadolsky *et al.*, Phys. Rev. D **78** (2008) 013004 [arXiv:0802.0007 [hep-ph]].
[18] A. D. Martin, W. J. Stirling, R. S. Thorne and G. Watt, arXiv:0901.0002 [hep-ph].
[19] S. Alekhin, K. Melnikov and F. Petriello, Phys. Rev. D **74** (2006) 054033 [arXiv:hep-ph/0606237].
[20] R. D. Ball *et al.* [NNPDF Collaboration], Nucl. Phys. B **809** (2009) 1 [Erratum-ibid. B **816** (2009) 293] [arXiv:0808.1231 [hep-ph]].
[21] B. C. Reisert [ZEUS Collaboration], arXiv:0809.4946 [hep-ex].
[22] G. Watt, JHEP **1109** (2011) 069 [arXiv:1106.5788 [hep-ph]].
[23] Y. L. Dokshitzer, V. A. Khoze, S. I. Troian and A. H. Mueller, Rev. Mod. Phys. **60**, 373 (1988).
[24] B. R. Webber, Nucl. Phys. B **238** (1984) 492.
[25] G. Marchesini and B. R. Webber, Nucl. Phys. B **310** (1988) 461.

[26] G. Corcella *et al.*, JHEP **0101**, 010 (2001) [arXiv:hep-ph/0011363].
[27] B. Andersson, G. Gustafson, G. Ingelman and T. Sjostrand, Phys. Rep. **97** (1983) 31.
[28] T. Sjostrand, P. Eden, C. Friberg, L. Lonnblad, G. Miu, S. Mrenna and E. Norrbin, Comput. Phys. Commun. **135** (2001) 238 [arXiv:hep-ph/0010017].
[29] T. Sjostrand, S. Mrenna and P. Skands, JHEP **0605**, 026 (2006) [arXiv:hep-ph/0603175].
[30] S. Gieseke, A. Ribon, M. H. Seymour, P. Stephens and B. Webber, JHEP **0402** (2004) 005 [arXiv:hep-ph/0311208].
[31] G. Aad *et al.* [ATLAS Collaboration], Phys. Rev. D **85** (2012) 072004 [arXiv:1109.5141 [hep-ex]].
[32] S. Chatrchyan *et al.* [CMS Collaboration], Phys. Rev. Lett. **107** (2011) 132001 [arXiv:1106.0208 [hep-ex]].
[33] E. Eichten, K. D. Lane and M. E. Peskin, Phys. Rev. Lett. **50** (1983) 811.
[34] G. Aad *et al.* [ATLAS Collaboration], New J. Phys. **13** (2011) 053044 [arXiv:1103.3864 [hep-ex]].
[35] G. Aad *et al.* [ATLAS Collaboration], Phys. Rev. D **85** (2012) 092002 [arXiv:1201.1276 [hep-ex]].